

# Early stages of the shear banding instability in wormlike micelles

S. M. Fielding\* and P. D. Olmsted†  
*Polymer IRC and Department of Physics & Astronomy,  
 University of Leeds, Leeds LS2 9JT, United Kingdom*

(Dated: October 29, 2018)

We study the early stages of the shear banding instability in semidilute wormlike micelles using the non-local Johnson-Segalman model with a two-fluid coupling of the concentration  $\phi$  to the shear rate  $\dot{\gamma}$  and micellar strain  $\underline{W}$ . We calculate the “spinodal” limit of stability for sweeps along the homogeneous intrinsic flow curve. For startup “quenches” into the unstable region, the instability in general occurs before the homogeneous startup flow can attain the intrinsic flow curve. We predict the selected time and length scales at which inhomogeneity first emerges. In the “infinite drag” limit, fluctuations in the mechanical variables  $\dot{\gamma}$  and  $\underline{W}$  are independent of those in  $\phi$ , and are unstable when the slope of the intrinsic flow curve is negative; but no length scale is selected. For finite drag, the mechanical instability is enhanced by coupling to  $\phi$  and a length scale is selected, in qualitative agreement with recent experiments. For systems far from an underlying zero-shear demixing instability this enhancement is slight, while close to demixing the instability sets in at low shear rates and is essentially demixing triggered by flow.

PACS numbers: 47.50.+d Non-Newtonian fluid flows– 47.20.-k Hydrodynamic stability– 36.20.-r Macromolecules and polymer molecules

Control of morphology and stability is vital for processing many complex fluids, *e.g.* polymeric, liquid crystalline, and surfactant fluids. While much is understood close (or relaxing) to equilibrium, strongly driven systems suffer in comparison. For many complex fluids, the intrinsic constitutive curve of shear stress  $\Sigma$  versus shear rate  $\dot{\gamma}$  is non-monotonic. For semi-dilute wormlike micelles, theory predicts the form ACEG of Fig. 1 [1, 2]. In the regime of decreasing stress,  $\dot{\gamma}_{c1} < \dot{\gamma} < \dot{\gamma}_{c2}$ , homogeneous flow is unstable [3, 4] and the system splits into bands of different shear rates  $\dot{\gamma} = \dot{\gamma}_\ell, \dot{\gamma}_h$  [6, 7, 8, 9, 10], with a steady state flow curve ABFG. Constitutive models augmented with interfacial gradient terms have captured this behaviour [5, 12]. In this paper we study the linear stability of initially homogeneous states. We also predict the length and time scales at which inhomogeneity emerges after a startup “quench”, *i.e.* imposing a shear rate in the unstable regime. Our analysis is the counterpart, for this *driven* phase transition, of the Cahn-Hilliard (CH) calculation for demixing in *undriven* systems.

Shear startup experiments [8, 13, 14] reveal (i) a metastable regime  $\dot{\gamma}_\ell < \dot{\gamma} \lesssim \dot{\gamma}_{c1}$  of slow approach to the banded state, and (ii) an unstable regime, onset at  $\dot{\gamma} \gtrsim \dot{\gamma}_{c1}$ , where the stress can massively overshoot  $\Sigma_{sel}$  before subsiding rapidly to it. In Ref. [14], the overshoot coincided with concentration fluctuations that emerged perpendicular to the shear compression axis at a selected length scale  $O(1\mu\text{m})$ . The authors attributed this to the Helfand-Fredrickson (HF) [15] coupling of flow to

concentration. This features in two component systems with well separated relaxation times (*e.g.* polymer and solvent) [15, 16, 17, 18, 19, 20]. The slow component (polymer) tends to migrate to regions of high stress. If the plateau modulus increases with polymer concentration, positive feedback enhances concentration fluctuations and can shift the spinodal of any nearby CH instability[20].

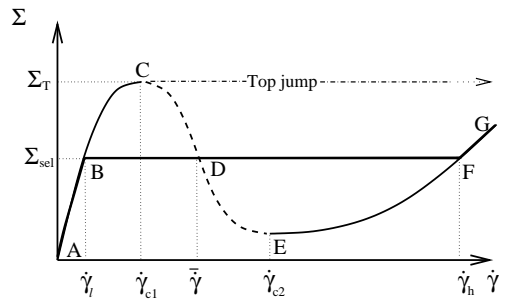


FIG. 1: Schematic flow curve.

Here we model the initial stage of the unstable kinetics using the non-local Johnson-Segalman (d-JS) model [22] within a 2-fluid framework [16, 18] that incorporates concentration dynamics. The 2-fluid model considers separate force balance equations for the micelles (velocity  $\underline{v}_m$ , volume fraction  $\phi$ ) and solvent (velocity  $\underline{v}_s$ ). These are added to give overall force balance for the average velocity  $\underline{v} = \phi \underline{v}_m + (1 - \phi) \underline{v}_s$  (Eq. 1) and subtracted for the relative velocity  $\underline{v}_{rel} = \underline{v}_m - \underline{v}_s$ , which in turn specifies the concentration fluctuations (Eq. 2):

$$\rho(\partial_t + \underline{v} \cdot \underline{\nabla}) \underline{v} \equiv D_t \underline{v} = \underline{\nabla} \cdot G(\phi) \underline{W} - \phi \underline{\nabla} \frac{\delta F(\phi)}{\delta \phi} + 2 \underline{\nabla} \cdot \phi \eta_m \underline{D}_m^0 + 2 \underline{\nabla} \cdot (1 - \phi) \eta_s \underline{D}_s^0 - \underline{\nabla} p, \quad (1)$$

$$D_t \phi = - \underline{\nabla} \cdot \phi(1 - \phi) \underline{v}_{\text{rel}} = - \underline{\nabla} \cdot \frac{\phi^2(1 - \phi)^2}{\zeta(\phi)} \left[ \frac{\underline{\nabla} \cdot G(\phi) \underline{W}}{\phi} - \underline{\nabla} \frac{\delta F}{\delta \phi} + \frac{2 \underline{\nabla} \cdot \phi \eta_m \underline{D}_m^0}{\phi} - \frac{2 \underline{\nabla} \cdot (1 - \phi) \eta_s \underline{D}_s^0}{1 - \phi} \right]. \quad (2)$$

$G(\phi) \underline{W}$  is the viscoelastic micellar backbone stress,  $W_{\alpha\beta} = \frac{\partial R'_\alpha}{\partial R} \cdot \frac{\partial R'_\beta}{\partial R} - \delta_{\alpha\beta}$  is the local strain that would have to be reversed to relax this stress, and  $G$  is the plateau modulus. The free energy  $F$  comprises osmotic and elastic parts:

$$F = \frac{1}{2} \int d^3q (1 + \xi^2 q^2) f'' |\phi(q)|^2 + \frac{1}{2} \int d^3x G(\phi) \text{tr}[\underline{W} - \log(\underline{\delta} + \underline{W})], \quad (3)$$

where  $f''$  is the osmotic susceptibility and  $\xi$  the equilibrium correlation length for concentration fluctuations. The Newtonian stress  $2\phi \eta_m \underline{D}_m^0$  describes fast micellar processes (*e.g.* Rouse modes) with  $\underline{D}_m^0$  the traceless symmetric micellar strain rate tensor, and  $2(1 - \phi) \eta_s \underline{D}_s^0$  is the solvent stress. Incompressibility determines the pressure  $p$ . The drag coefficient  $\zeta$  (Eq. 2) ensures that the force  $\zeta \underline{v}_{\text{rel}}$  impedes relative motion. The micellar diffusion coefficient  $D \propto f''/\zeta$ . We have omitted negligible inertial corrections to Eqs. (1) and (2) [21].

Eq. (1) is the Navier Stokes equation generalised to include osmotic stresses. Eq. (2) is a generalised CH equation in which micelles diffuse in response to gradients in the osmotic force  $\underline{\nabla}[\delta F/\delta \phi]$  and in the viscoelastic stress; for  $dG/d\phi > 0$  (assumed here), HF feedback occurs. The micellar strain obeys d-JS dynamics [22]:

$$(\partial_t + \underline{v}_m \cdot \underline{\nabla}) \underline{W} = a(\underline{D}_m \cdot \underline{W} + \underline{W} \cdot \underline{D}_m) + (\underline{W} \cdot \underline{\Omega}_m - \underline{\Omega}_m \cdot \underline{W}) + 2 \underline{D}_m - \frac{\underline{W}}{\tau(\phi)} + \frac{l^2}{\tau(\phi)} \underline{\nabla}^2 \underline{W} \quad (4)$$

where  $2 \underline{\Omega}_m = \underline{\nabla} \underline{v}_m - (\underline{\nabla} \underline{v}_m)^T$  with  $(\underline{\nabla} \underline{v}_m)_{\alpha\beta} \equiv \partial_\alpha (v_m)_\beta$ .  $\tau(\phi)$  is the Maxwell time;  $l$  is a length that could, for example, be set by the mesh-size. The slip parameter  $a$  measures the fractional stretch of the micelles compared to the flow. For  $|a| < 1$  (slip) the intrinsic flow curve  $\Sigma_{xy}(\dot{\gamma})$  is capable of the non-monotonicity of Fig. 1.

We study planar shear between infinite plates at  $y = \{0, L\}$  with  $(\underline{v}, \underline{\nabla} v, \underline{\nabla} \wedge \underline{v})$  in the  $(\hat{x}, \hat{y}, \hat{z})$  directions. At the plates we assume  $\partial_y \phi = \partial_y^3 \phi = 0$ ,  $\partial_y \underline{W} = 0$ , and no slip. For controlled strain rate (assumed throughout)  $\int_0^L dy \dot{\gamma}(y) = \text{const}$ . Unless stated, we use model parameter values at  $\phi = 0.11$  from rheological data for CTAB(0.3M)/NaNO<sub>3</sub>/H<sub>2</sub>O [24], and light scattering (DLS) data for CTAB/KBr/H<sub>2</sub>O [25]; we calculate the drag as  $\zeta = 6\pi\bar{\eta}\xi^{-2}$  [23] where  $\bar{\eta} = \phi\eta_m + (1 - \phi)\eta_s$ . We extrapolate  $G(\phi)$ ,  $\tau(\phi)$ ,  $D(\phi)$ ,  $\zeta(\phi)$ ,  $\xi(\phi)$  to  $\phi < 0.11$  using scaling laws for semidilute wormlike micelles. We fix  $a$  (assumed independent of  $\phi$ ) by comparing with Cates' model [1]; and use units in which  $G(\phi = 0.11) = 1$ ,  $\tau(\phi = 0.11) = 1$  and  $L = 1$ . The homogeneous intrinsic flow curves  $\Sigma_{xy}(\dot{\gamma}, \phi)$  that satisfy  $\partial_t \underline{v} = \partial_t \phi = \partial_t \underline{W} = 0$  are shown as dashed lines in Fig. 2. The region of negative slope ends at a ‘‘critical’’ point  $\phi_c \approx 0.015$ : CPCl/NaSal in brine [8] shows the same trend.

We linearise in fluctuations  $\sum_{\underline{k}} [\delta \dot{\gamma}, \delta \underline{W}, \delta \phi]_{\underline{k}} e^{i\underline{k} \cdot \underline{r} + \omega t}$  about these homogeneous states. The stability analysis  $\omega_{\underline{k}, \alpha} \underline{v}_{\underline{k}, \alpha} = \underline{M}_{\underline{k}} \underline{v}_{\underline{k}, \alpha}$  gives the normal modes  $\underline{v}_{\underline{k}, \alpha}$  (where  $\alpha$  is the mode index), each encoding a set of relative amplitudes of  $\delta \dot{\gamma}$ ,  $\delta W_{ij}$ ,  $\delta \phi$ . The lower spinodal lies where

the largest branch  $\omega_{\underline{k}}$  of the dispersion relation first goes positive (unstable) as the background homogeneous state is swept up the intrinsic flow curve from  $\dot{\gamma} = 0$ ; the upper spinodal is defined likewise, for sweeps down from large  $\dot{\gamma}$ . We consider only  $\underline{k} = k\hat{y}$ ; the stability of  $\underline{k} = k\hat{z}$  is unaffected by shear in our model.

In the limit of infinite drag  $\zeta \rightarrow \infty$  at fixed  $\underline{\nabla} \cdot \frac{1}{\zeta} \underline{\nabla} \frac{\delta F}{\delta \phi}$ , the coupling of  $\delta \dot{\gamma}$  and  $\delta \underline{W}$  to  $\delta \phi$  is disabled. Fluctuations in the mechanical subspace  $[\delta \dot{\gamma}, \delta W_{xy}, \delta W_{xx}, \delta W_{yy}]$  then obey conventional (uniform- $\phi$ ) d-JS dynamics, in which any homogeneous shear state in the regime of negative constitutive slope  $d\Sigma_{xy}/d\dot{\gamma} < 0$  is unstable: the spinodal is given by circles in Fig. 2. The concentration fluctuations independently obey conventional (zero-shear) CH dynamics, with a demixing instability when  $D < 0$ . We consider only *flow-induced* instabilities here,  $D > 0$ .

For finite drag, HF feedback couples these subspaces and can induce instability even if  $d\Sigma_{xy}/d\dot{\gamma} > 0$  and  $D > 0$ . For model parameters from the data of Refs. [24, 25], the mechanical instability is enhanced slightly by concentration coupling (squares in Fig. 2). This effect increases near a zero-shear demixing instability: see the diamonds and triangles in Fig. 2, for smaller  $D(\phi = 0.11)$ . (The lobe of instability at high shear rate is discussed in Ref. [21].) Within some simplifying assumptions [21], a qualitative expression for the lower spinodal is  $\tilde{D} \frac{d\Sigma_{xy}}{d\dot{\gamma}} + \frac{dG}{d\phi} \frac{W_{xy}}{\zeta} \frac{dZ}{d\dot{\gamma}} = 0$  where  $2Z = (a - 1)W_{xx} + (a + 1)W_{yy} < 0$ ,  $\tilde{\zeta} \propto \zeta$  and  $\tilde{D} = D - \frac{dG}{d\phi} \frac{Z}{\zeta}$ .

Enhancement of flow instabilities by positive feedback

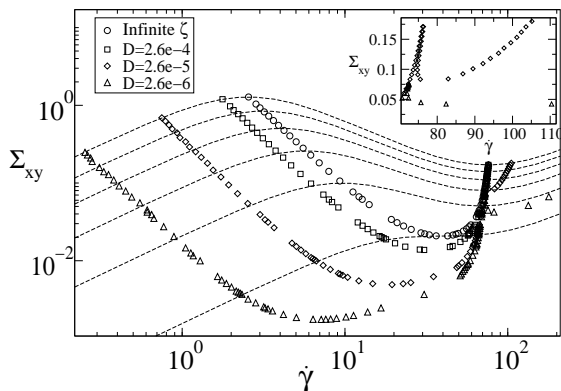


FIG. 2: Dashed lines: intrinsic flow curves for  $\phi = 0.11, 0.091, 0.072, 0.053, 0.034, 0.015$  (downwards). Symbols: spinodals for the uncoupled limit  $\zeta \rightarrow \infty$  ( $\circ$ ); coupled model with  $D(\phi = 0.11)$  taken from DLS ( $\square$ ); coupled model with artificially reduced  $D$  ( $\diamond, \triangle$ ). Inset: zoom on large  $\dot{\gamma}$ .

with concentration was first predicted by the remarkable insight of Schmitt *et al.*[26]. However they directly assumed a chemical potential  $\mu = \mu(\dot{\gamma})$ . Although this is equivalent to our approach in the limit of adiabatic stress response (assumed in [26]), below we find that the dynamics inside the spinodal *are* dictated by the micellar stress response. The spinodal is unaffected since the dynamics are adiabatic here by definition: the above condition corresponds to Schmitt's Eq. (24).

Experimentally the spinodal is found via sweeps along the intrinsic flow curve, though in practice banding can occur prematurely via metastable kinetics [13]. The same ambiguity arises in the spinodal of conventional fluid-vapour demixing, defined via quasistatic compression.

We now study the early-time kinetics in the unstable regime. We cannot assume that the system starts in a homogeneous state on the unstable intrinsic flow curve, since the Maxwell time  $\tau$  needed to prepare such a state is longer than the typical time scales  $1/\omega_k$  of the instability itself (except very near the spinodal) [28], and so most startup flows go unstable before the intrinsic

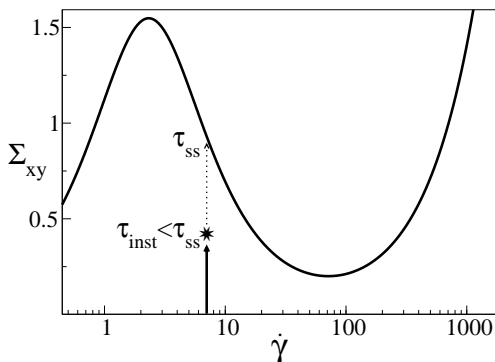


FIG. 3: Instability occurring as the homogeneous startup flow evolves towards the intrinsic unstable constitutive curve.

flow curve can be attained. When the rheometer plate is first set moving the shear rate rapidly homogenises,

on the Reynolds timescale  $\rho L^2/\eta \ll \tau$ . The shear stress  $\Sigma(t) = G\underline{W}(t) + \eta\dot{\gamma}$  then *starts* to evolve towards the intrinsic flow curve, with  $\underline{W}(t)$  *initially* given by the homogeneous startup solution of Eq. (4). Without noise, it would attain this flow curve at some time  $\tau_{ss} = O(\tau)$ . But of course the system has noise. The stability problem is now time-dependent:  $\omega_{k,\alpha}(t)\underline{v}_{k,\alpha}(t) = \underline{M}_k(t)\underline{v}_{k,\alpha}(t)$  since  $\underline{M}_k = \underline{M}_k(\dot{\gamma}, \underline{W}(t), \phi)$ . At first all dispersion branches are stable. Then at some time  $t_0 \leq \tau_{ss}$  a branch goes unstable. The size of the growing fluctuations at  $t > t_0$  is  $A_k(t) \sim \exp\left[\int_{t_0}^t dt' \omega_k(t')\right]$ . A rough criterion for detectability is  $\log A = O(10)$ , which defines a  $k$ -dependent time scale  $\tau_{\text{inst}}(k)$  via  $\int_{t_0}^{\tau_{\text{inst}}(k)} dt' \omega_k(t') = O(10)$ . In most regimes, fluctuations emerge fastest at a selected wavevector  $k^*$ , because of a peak in the dispersion relation  $\omega_k(t)$  (Fig. 4). We thus define the overall time scale of the instability to be  $\tau_{\text{inst}} = \tau_{\text{inst}}(k^*)$  (Fig. 3).

Fig. 4 gives the unstable dispersion branch  $\omega_k(t)$  and the eigenvector at the maximum in  $\omega_k$  for three startup flows.  $\tau_{\text{inst}}$  is marked in each case. (We used a continuous  $k$  axis though in practice only harmonics  $k = n\pi$  are allowed.) For the pure mechanical instability ( $\zeta \rightarrow \infty$ , Fig. 4(a)),  $\omega_k$  is cut off at large  $k$  by interfaces and at low  $k$  (beyond the gap size) by Reynolds effects. Between there is a plateau where  $\omega_k$  is set by the viscoelastic stress response, with no clearly selected lengthscale. Fig. 4(b) is for a coupled model far from a zero-shear CH demixing instability (with the spinodal given by circles in Fig. 2). Concentration coupling has enhanced the mechanical instability at short length scales; in competition with the interfacial terms this selects a length scale  $k^{*-1}$ , as seen experimentally [14]. The eigenvector at  $k^*$  (Fig. 4(b), bottom) is mainly still in the  $\delta\dot{\gamma}$  and  $\delta\underline{W}$  directions, as expected. The plateau of the mechanical instability is still apparent at smaller  $k$ , since this shear rate would have been unstable even for  $\zeta \rightarrow \infty$ . Concentration diffusion cannot keep pace at these length scales, and is absent from the eigenvector. Fig. 4(c) is for a system close to zero-shear demixing, for which the lower spinodal is at a shear rate far below the spinodal of the pure mechanical instability (triangles in Fig. 2). Our imposed shear rate is just inside this spinodal, so the mechanical plateau is absent from the dispersion relation, leaving only the diffusive concentration-coupled branch. The eigenvector is dominated by  $\delta\phi$ , so this instability is essentially demixing, triggered by flow. It occurs slowly enough that the intrinsic flow curve is reached before fluctuations grow appreciably:  $\tau_{\text{inst}}$  is off the scale of Fig. 4(c).

In summary, we have studied the early time kinetics of the shear banding instability in the d-JS model with 2-fluid coupling to concentration. The spinodal onset of pure mechanical instability with negative constitutive slope  $d\Sigma_{xy}/d\dot{\gamma} < 0$  (mathematically indistinguishable from a flow-induced transition in, for example, nematic liquid crystals [27]) is shifted by coupling to concentration. For startup quenches deep in the unstable

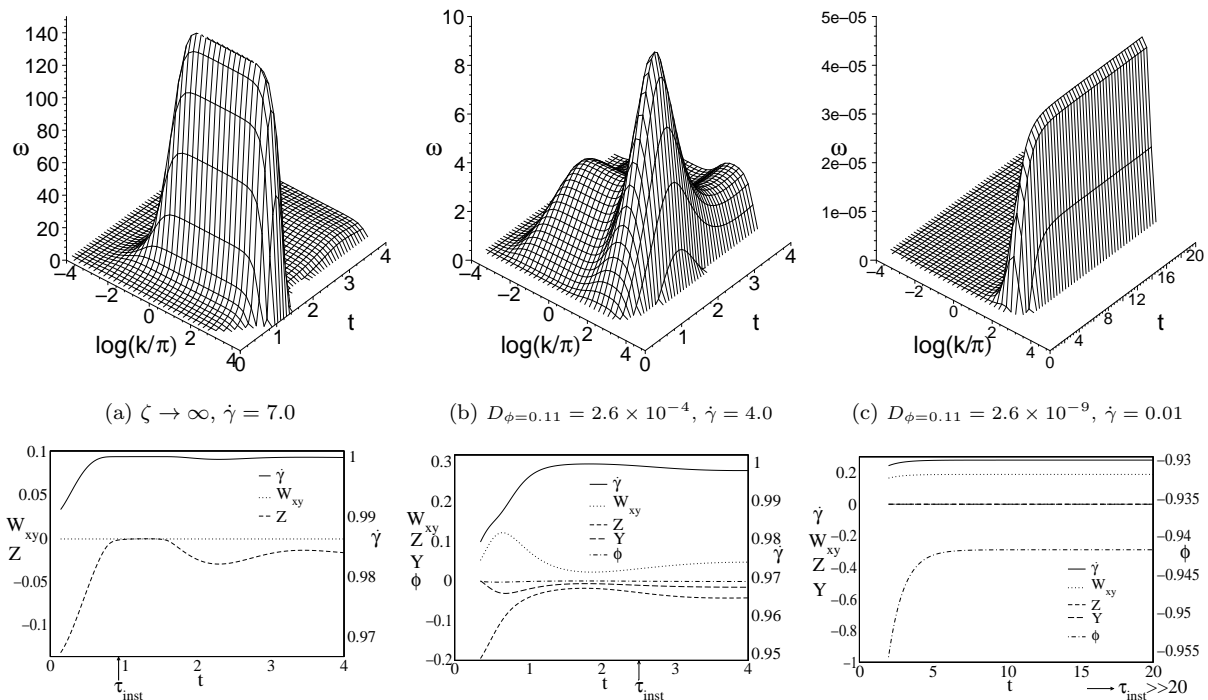


FIG. 4: Startup dispersion relation  $\omega_k$  (top) and eigenvector at max. in  $\omega_k$  (bottom).  $Z = \frac{1}{2}(a-1)W_{xx} + \frac{1}{2}(1+a)W_{yy}$ ;  $Y = \frac{1}{2}(1-a)W_{xx} - \frac{1}{2}(1+a)W_{yy}$ .

region the instability in general occurs before the homogeneous startup flow can attain the intrinsic flow curve. An initial length scale is selected only if the instability is coupled to concentration. These results are qualitatively consistent with recent experiments on wormlike micellar solutions [24].

**Acknowledgments** We thank Paul Callaghan, Ron Larson, Sandra Lerouge, and Tom McLeish for interesting discussions and EPSRC GR/N 11735 for financial support; this work was supported in part by the National Science Foundation under Grant No. PHY99-07949.

\* Electronic address: physf@irc.leeds.ac.uk

† Electronic address: p.d.olmsted@leeds.ac.uk

- [1] M. E. Cates, *J. Phys. Chem.* **94**, 371 (1990).
- [2] N. A. Spenley and M. E. Cates, *Macromolecules* **27**, 3850 (1994). N. A. Spenley, X.-F. Yuan, and M. E. Cates, *J. Phys. II (Fr)* **6**, 551 (1996).
- [3] J. Yerushalmi, S. Katz, and R. Shinnar, *Chemical Engineering Science* **25**, 1891 (1970).
- [4] N. A. Spenley, M. E. Cates, and T. C. B. McLeish, *Phys. Rev. Lett.* **71**, 939 (1993).
- [5] J. K. G. Dhont, *Phys. Rev.* **E 60**, 4534 (1999). X.-F. Yuan, *Europhys. Lett.* **46**, 542 (1999).
- [6] H. Rehage and H. Hoffmann, *Mol. Phys.* **74**, 933 (1991).
- [7] J. F. Berret, D. C. Roux, G. Porte, and P. Lindner, *Europhys. Lett.* **25**, 521 (1994). V. Schmitt, F. Lequeux, A. Pousse, and D. Roux, *Langmuir* **10**, 955 (1994).
- [8] J. F. Berret, D. C. Roux, and G. Porte, *J. Phys. II (France)* **4**, 1261 (1994).
- [9] R. Makhoulfi, J. P. Decruppe, A. Aitali, and R. Cressely, *Europhys. Lett.* **32**, 253 (1995). J. P. Decruppe, E. Cappelaere, and R. Cressely, *J. Phys. II (France)* **7**, 257 (1997). J. F. Berret, G. Porte, and J. P. Decruppe, *Phys. Rev.* **E 55**, 1668 (1997).
- [10] R. W. Mair and P. T. Callaghan, *Europhys. Lett.* **36**, 719 (1996); *J. Rheol.* **41**, 901 (1997). M. M. Britton and P. T. Callaghan, *Phys. Rev. Lett.* **78**, 4930 (1997).
- [11] J. F. Berret, D. C. Roux, and P. Lindner, *European Physical Journal B* **5**, 67 (1998).
- [12] C.-Y. D. Lu, P. D. Olmsted, and R. C. Ball, *Phys. Rev. Lett.* **84**, 642 (2000). P. D. Olmsted and P. M. Goldbart, *Phys. Rev.* **A46**, 4966 (1992). J. R. A. Pearson, *J. Rheol.* **38**, 309 (1994).
- [13] J. F. Berret, *Langmuir* **13**, 2227 (1997). C. Grand, J. Arrault, and M. E. Cates, *J. Phys. II (France)* **7**, 1071 (1997). S. Lerouge, J. P. Decruppe, and C. Humbert, *Phys. Rev. Lett.* **81**, 5457 (1998). S. Lerouge, J. P. Decruppe, and J. F. Berret, *Langmuir* **16**, 6464 (2000). J. F. Berret and G. Porte, *Phys. Rev.* **E 60**, 4268 (1999).
- [14] J. P. Decruppe, S. Lerouge, and J. F. Berret, *Phys. Rev. E* **6302**, 2501 (2001).
- [15] E. Helfand and G. H. Fredrickson, *Phys. Rev. Lett.* **62**, 2468 (1989).
- [16] P.-G. de Gennes, *Macromolecules* **9**, 587 (1976). F. Brochard, *J. Phys. (Paris)* **44**, 39 (1983).
- [17] M. Doi and A. Onuki, *J. Phys. II (France)* **2**, 1631 (1992).
- [18] S. T. Milner, *Phys. Rev.* **E48**, 3674 (1993); *Phys. Rev. Lett.* **66**, 1477 (1991).
- [19] X. L. Wu, D. J. Pine, and P. K. Dixon, *Phys. Rev. Lett.*

- 66**, 2408 (1991).
- [20] N. Clarke and T. C. B. McLeish, Phys. Rev. **E 57**, R3731 (1998). T. Sun and A. C. Balazs and D. Jasnow, Phys. Rev. **E 55**, R6344 (1997).
- [21] S M Fielding and P D Olmsted. In preparation.
- [22] M. Johnson and D. Segalman, J. Non-Newt. Fl. Mech **2**, 255 (1977). P. D. Olmsted, O. Radulescu, and C.-Y. D. Lu, J. Rheology **44**, 257 (2000).
- [23] P. G. de Gennes, *Scaling Concepts in Polymer Physics* (Cornell, Ithaca, 1975).
- [24] S Lerouge. PhD Thesis, University of Metz, 2000.
- [25] S. J. Candau, E. Hirsch, and R. Zana, J. Colloid Interface Sci. **105**, 521 (1985).
- [26] V. Schmitt, C. M. Marques, and F. Lequeux, Phys. Rev. **E52**, 4009 (1995).
- [27] P. D. Olmsted and C.-Y. D. Lu, Phys. Rev. **E60**, 4397 (1999).
- [28] For temperature quenches in CH demixing, the system essentially starts on the unstable branch of the chemical potential because heat-conduction is fast enough to effect the quench before demixing starts.